2024, 21(5): 1684-1691
https://dx.doi.org/10.21123/bsj.2023.8327
P-ISSN: 2078-8665 - E-ISSN: 2411-7986
Baghdad Science Journal

Influence of pulse laser energy on the Nickel plasma characteristics that produced in laser-induced plasma system

Sabah N. Mazhir*, *Huda H. Abbas*

Department of Physics, College of Science for Women, University of Baghdad. Iraq.
*Corresponding Author.

Received 05/01/2023, Revised 23/04/2023, Accepted 25/04/2023, Published Online First 20/10/2023, Published 01/05/2024

Abstract

Optical Emission Spectrometry technique (OES) is used to analyze the plasma generated from a (Ni) target illuminated with a Q- Switched (Nd:YAG) laser at various energies in the air. Boltzmann-Plot and Stark broadening methods were used to calculate the plasma parameters including electron density (n_e), electron temperature (T_e), plasma frequency (fp), and Debye length (λ_D). It is shown that the values of (n_e), (T_e), (λ_D) and (fp) increase with increasing laser energy with the calculated electron temperature values ranging between 0.934 - 1.479 eV.

Keywords: Debye length, Electron Temperature, Nickle, Optical Emission Spectrometry technique, Plasma.

Introduction

The term "laser-induced plasma spectroscopy (LIPS)" refers to an atomic emission spectroscopy method that makes use of high-energy laser pulses to excite atoms in materials[1]. High-power laser interactions with the matter may result in the formation of transitory plasma. Laser- induced breakdown spectroscopy (LIBS), which depends on laser-plasma atomic emission spectroscopy is a novel method of elemental analysis, that possesses several advantageous characteristics[2]. They include high resolution, nearly nondestructive measurement of the target, the ability to analyze multiple elements in real-time online at the same time, and the ability to be applied to solid, liquid, gas, and aerosol materials[3]. LIBS can achieve both qualitative and quantitative analysis of the target material, and as a result, the technique is extensively used in environmental pollution monitoring, diamond jewelry evaluation, and industrial manufacturing[4,5].

In addition to laser properties such as wavelength, pulse energy, and pulse width; the nature of the target material and the surrounding environment; as well as the measuring equipment, are factors that can impact LIBS [6-7]. As a result of these factors, the repeatability of the LIBS signal is low, which is one of the key challenges that hamper the deployment of LIBS technology[8,9]. The study of hardware improvement, as well as research into the system through experiment equipment, measurement environment, optimizing target material properties, and other methods of improving the accuracy of experimental data have been conducted to overcome matrix effects and improve the accuracy of experimental data[10]. It has thus become a significant research trend to increase the dependability and stability of LIBS technology by improving the spectrum of data processing as a result of these considerations [11-12]. The purpose of this research is to

2024, 21(5): 1684-1691
https://dx.doi.org/10.21123/bsj.2023.8327
P-ISSN: 2078-8665 - E-ISSN: 2411-7986
Baghdad Science Journal

evaluate the effects of laser pulse energy on Ni plasma in the characterization of the air at atmospheric pressure.

Experimental LIBS setup

The LIBS experimental setup is depicted schematically in Fig 1**,** The tests were carried out at room temperature and air. Nickle samples were chosen for plasma production, and the Ni target purity was nearly 99.9999%. The plasma was generated using a Q - switched nanosecond laser source, which has an essential wavelength of 1064 nm, a pulse duration of 10 ns, and a repeating frequency of 6 Hz for the laser. The distance from the spectrometer to the laser target is around 30 cm. The laser-induced plasma light emission from the Ni target surface was captured using an optical fiber with a 50 µm diameter core that was positioned at a 1 cm distance from the Ni target surface. NIST database software [13] was used to assign the optical emission line to specified elements to determine the plasma properties.

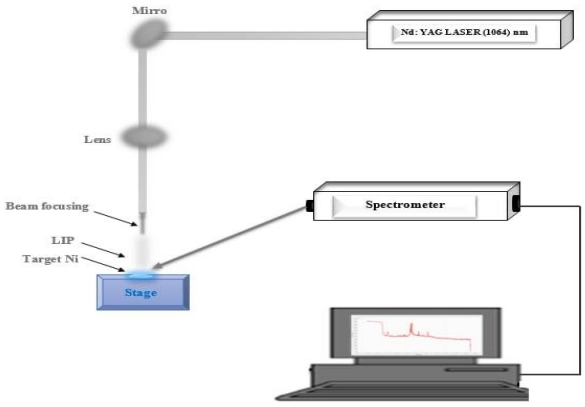

Figure 1. Schematic diagram of the experimental setup for LIBS.

Results and Discussion

Spectra of Ni plasma

The radiation spectrum of Ni plasma at wavelengths ranging from 200 nm to 1000 nm is depicted in Fig 2. Several nickel emission lines (such as Ni I at 286.55 nm, 366.40 nm, 385.83 nm, 440.15 nm, 446.24 nm, 460.5 nm, 471.57 nm, 485.54 nm, 508.40 nm, and 547.08 nm, among others) are superimposed over continuous background radiation. This result can be explained according to Singh[14], if sufficiently high energy applied to the atom (overcoming ionization potential) is available, the atom's electrons can be separated from its atom, which creates free electrons and positive ions. The atom's electrons separate is the most external (the most distant in relation to the nucleus) since it has the lowest ionization energy. However, more electrons can be separated with a higher energy supply. The most frequency of these ions is photons during the recombination phase (ions absorb free electrons in the process known as a free-bound transition) or in the process of deexcitation (in a process called free transition via the kinetic method, ions and electrons lose their energy). The different ion energies and energy transitions can cause these emissions to be a continuum. Furthermore, ion deexcitation has a discrete (or quantized) set of energy levels with characteristic emission lines for each type, which allow for identification with atomic emission lines[15]. The correlation data of the atomic spectral standard and the technical database from the National Institute of Standards and Technology (NIST) as well as the spectral line analysis software from the spectrometer have been used to identify the nickel atom spectrum in Fig 2, their flat regions in the spectra of 400 and 500mJ at 200-260nm and 300-370nm the reason is that our optical fiber spectrometer was not sensitive enough for detection and not sufficiently capable of distinguishing the peaks of the elements.

2024, 21(5): 1684-1691
https://dx.doi.org/10.21123/bsj.2023.8327
P-ISSN: 2078-8665 - E-ISSN: 2411-7986
Baghdad Science Journal

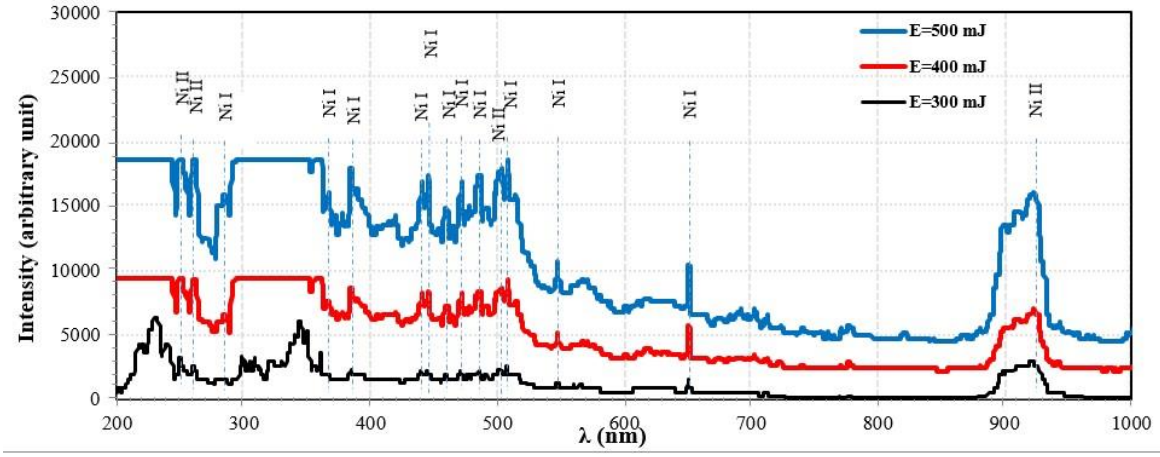

Figure 2. The plasma emission spectra of Ni target as a function of energy at laser energy 400, 500, and 600 mJ in air.

Electron temperature in laser-induced Ni plasma

In plasma, the electron temperature and the electron number density are two fundamental thermodynamic characteristics that must be considered. Only when the plasma is under Local Thermodynamic Equilibrium (LTE) does the temperature of the plasma have physical relevance [15]. When the plasma is in LTE, the electron temperature may be used to define the key plasma properties. For example, in the LTE, particle velocities have Maxwellian distribution, while particle numbers in different energy levels are distributed in accordance with the Boltzmann distribution. The adjacent ionization state of a single particle is distributed in accordance with the Saha equation. As predicted by the Boltzmann distribution of particles, the spectral line intensity Iji and the spectral energy Ej associated with the higher level are both met in the following ways [16].

$$\ln\left[\frac{I_{ji}\,\lambda}{hcg_j\,A_{ji}}\right] = -\frac{1}{kT_e}\,E_j + \ln\left[\frac{N}{4\pi\,U}\right] \quad \ldots\ldots 1$$

For each level, A_{ji} denotes the transition probability, gj indicates the statistical weight of the higher level, h denotes planck constant, and c denotes the speed of light in a vacuum. E_j is the energy at the top level, in this equation, T_e is the temperature of the electrons, k is the Boltzmann constant, U is a partition function, and N is the total number density of species, all in degrees Celsius.

It is possible to obtain the plasma temperature without knowing N or U if the vertical coordinate is $\ln\left[\frac{I_{ji}\,\lambda}{hcg_j\,A_{ji}}\right]$ and the horizontal coordinate is Ej, and the Boltzmann diagram is fitted in a linear manner. If the Boltzmann diagram is fitted in a linear manner, a line with a slope of $-\frac{1}{kT_e}$ is obtained. When attempting to solve the plasma temperature problem, it is necessary to know the excitation energy of the upper- level E_j, the degeneracy of the upper energy level g_j, and the spontaneous transition probability of the spectral lines A_{ji}, among other things. It has been shown that the literature estimates of the likelihood of spontaneous emission transition of the spectral lines A_{ji} are significantly different and that the measurement error of the spectral line intensity E_j is quite substantial[17]. As a result, the estimated plasma temperature of electrons will have a large inaccuracy, which will result in poor estimation of the other plasma characteristics.

As a result of advancements in the iterative Boltzmann technique, it is now possible to measure the electron temperature of laser-induced plasma. Because of the correlation coefficient of linear fitting of 0.6529 and the Boltzmann diagram (Fig 3) of the nickel atom line shown in Eq 1, the electron temperature of Ni plasma is determined to be 10,829.07 K as illustrated in Fig 4. The linear correlation coefficient of the line hits 0.8356 after 600 mJ laser energy of the Boltzmann method, according to the flow chart (Fig 5). In other words, based on the slope found above, the electron

2024, 21(5): 1684-1691
https://dx.doi.org/10.21123/bsj.2023.8327
P-ISSN: 2078-8665 - E-ISSN: 2411-7986
Baghdad Science Journal

temperature of the Ni plasma is 15,993.29K. Ni plasma's electron temperature remains constant between 15,993.29 K and 10,829.07 K throughout experimentation, increasing the linear fitting coefficient from 0.6529 to 0.8356. The value of the R factor is a statistical parameter that shows the extent to which the curve matches the specified points, and this means that it represents a measure of the accuracy of the curve, and its value must be confined between 0-1.

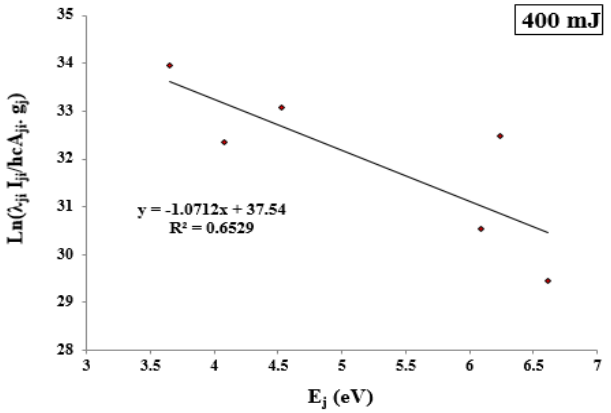

Figure 3. Local Boltzmann plot, the excitation energy of the upper- level as a function of transcendental function with a correlation coefficient of R2 =0.6529.

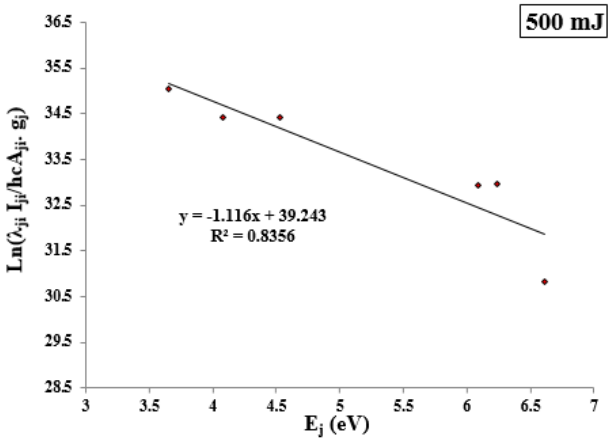

Figure 4. Local Boltzmann plot, the excitation energy of the upper- level as a function of transcendental function with a correlation coefficient of R^2 0.8356.

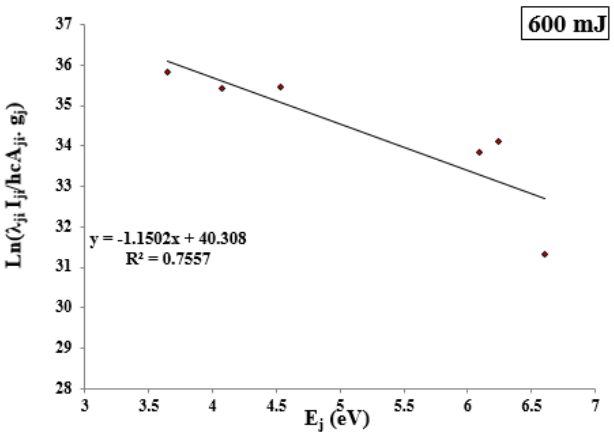

Figure 5. Local Boltzmann plot, the excitation energy of the upper- level as a function of transcendental function with a correlation coefficient of R^2 0.7557.

Table 1. Shows the physical characteristics of NI, NII lines.

Space	Wavelength (nm)	$A_{ji}.g_j$	E_i eV	E_k eV
Ni II	251.08	5.8 E8	1.68	6.61
Ni II	261.5	5.40E+06	1.68	6.39
Ni I	286.55	9.00E+06	0.21	4.53
Ni I	366.4	6.00E+06	0.27	3.65
Ni I	385.83	4.80E+07	0.42	3.63
Ni I	440.15	4.20E+08	3.19	6
Ni I	446.24	8.50E+07	3.46	6.24
Ni I	460.5	1.60E+08	3.47	6.17
Ni I	471.57	1.40E+08	3.54	6.17
Ni I	485.54	2.80E+08	3.54	6.09
Ni II	506.42	5.20E-03	1.15	3.6
Ni I	508.4	2.80E+08	3.67	6.11
Ni I	547.69	2.80E+07	1.82	4.08
Ni I	653.28	6.30E+04	1.93	3.82
Ni II	937.48	6.20E-05	0	1.32

Table 1. Lists the physical properties of the Ni I and Ni II lines the technical database from the National Institute of Standards and Technology (NIST) employed in this experiment.

Electron density in laser-induced Ni plasma

Stark broadening is the primary phenomenon by which the atomic emission line broadens in laser-induced plasma. This widening is driven by the surrounding charged particle field. The

2024, 21(5): 1684-1691
https://dx.doi.org/10.21123/bsj.2023.8327
P-ISSN: 2078-8665 - E-ISSN: 2411-7986
Baghdad Science Journal

following equations describe the connection between plasma electron number density and the Stark broadening breadth[17].

$$\Delta\lambda_{1/2} = 2\omega \left(\frac{N_e}{10^{16}}\right) + 3.5\, A \left(\frac{N_e}{10^{16}}\right)^{1/4} \left[1 - \frac{3}{4} N_D^{-\frac{1}{3}}\right] \omega \left(\frac{N_2}{10^{16}}\right) \quad \ldots\ldots 2$$

The contribution of electron widening is represented by the first term on the right of Eq 2, while the contribution of ion broadening is represented by the second term. $\Delta\lambda_{1/2}$ is Stark broadening the half peak width, ω is electron collision broadening coefficient, Ne is the number of electrons in the plasma, and N_D is the number of particles in the Debye ball, which may be represented as[18]:

$$N_D = 1.72 \times 10^9 \frac{T^{\frac{3}{2}}(eV)}{N_e^{\frac{1}{2}}(cm^{-3})} \quad \ldots\ldots 3$$

The widening of the ionic quasi-static coulomb field is a disruption in the laser-produced plasma, according to the Stark extension theory. Because the influence of electrons on radiation atoms is so important, the ion collision broadening may be neglected in the actual computation, ignoring the second item in Eq 2 as a result, the connection between Stark widening the half peak width and the number of plasma electrons may be simplified as follows[16].

$$\Delta\lambda_{1/2} = 2\,\omega \left(\frac{N_e}{10^{16}}\right) \quad \ldots\ldots 4$$

The Lorentz type Stark broadening spectral line has the following function expression[15].

$$y = y_\circ + \frac{2B}{\pi} \frac{\omega}{4(x - x_c)^2 + \omega^2} \quad \ldots\ldots 5$$

Where B is the spectral line's integral strength, is the whole width of the spectral line, X_c is the spectral line's center wavelength, and y_0 is the spectral line's background radiation intensity.

Fig 6 depicts the Stark broadening of Ni I 651.48 nm; the actual line is the Lorentz fitting curve, the square value of the correlation coefficient (R^2) is 0.83, and the spectral line's half-peak width is 0.35 nm. The plasma electron density of a Ni is 3.5 x 10^{18}cm^{-3}, according to the Stark broadening hypothesis, which ignores other broadening effects and deducts widening instrument situations by the relevant electron collision broadening coefficient [19]. Fig 7 variation of electron temperature and density in a laser-induced nickel plasma as a function of laser energy, the increase in plasma temperature may be due to the plasma becoming opaque to the laser beam that reaches the target, plasma shielding occurs when the plasma reduces the transmission of laser peak energy along the beam path. Table 2 lists the plasma parameters of the Ni lines with different laser energy. The saturation/slow variation of n and T_e was seen in the results. The behavior observed is related to the plasma shielding effect, i.e., plasma reflection of laser light. The ionization process is limited by the plasma shielding effect of air, reducing the efficiency of the available laser intensity for mass ablation.

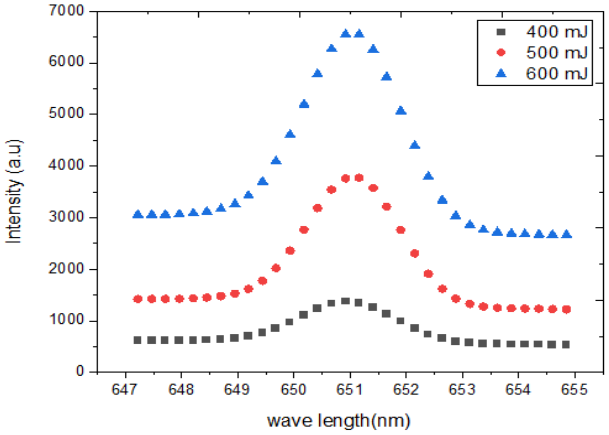

Figure 6. Stark broadening of Ni I (651.48) nm and Lorentz fitting

2024, 21(5): 1684-1691
https://dx.doi.org/10.21123/bsj.2023.8327
P-ISSN: 2078-8665 - E-ISSN: 2411-7986
Baghdad Science Journal

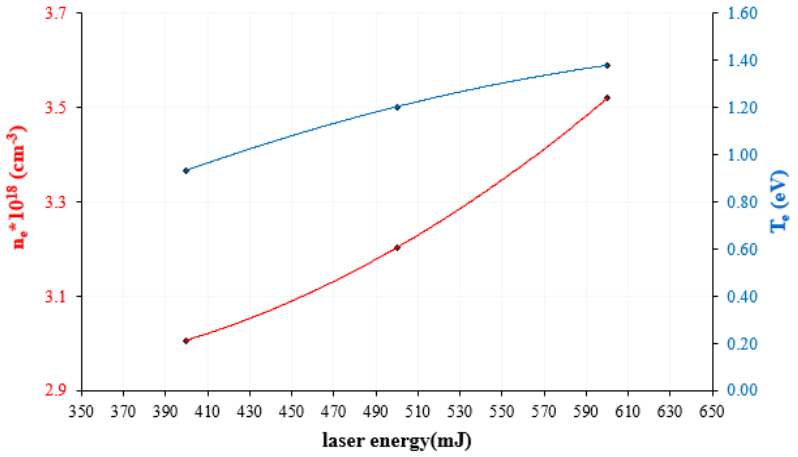

Figure 7. Variation of electron density of laser-induced nickel plasma and electron temperature with the laser energy

Table 2. Shows the plasma parameters of Ni with different laser energy.

Laser energy (mJ)	slope	R^2	T_e (eV)	$n_e \times 10^{18}$ (cm^{-3})	$\lambda_D \times 10^{-6}$ (cm)	$f_p \times 10^{13}$(Hz)
400	-1.05	0.65	0.934	3.030	4.124	1.563
500	-1.11	0.83	1.203	3.210	4.549	1.609
600	-1.15	0.755	1.379	3.500	4.663	1.680

Conclusion

Using optical emission spectroscopy (OES), the pulsed Q-switched Nd:YAG laser incident spectra are examined on a Ni target in the air at a fundamental wavelength of 1064 nm. The emission spectra of the plasma show multiple emission lines from the element Ni. The irradiance of the laser is used to model the plasma and estimate its characteristics. As the pulse energy of the laser gets higher, the higher temperature of the electrons will become and the density of the electrons will get higher. In addition, the plasma frequency, Debye length, rises as the laser light power increases.

Authors' Declaration

- Conflicts of Interest: None.
- We hereby confirm that all the Figures and Tables in the manuscript are ours. Furthermore, any Figures and images, that are not ours, have been included with the necessary permission for re-publication, which is attached to the manuscript.
- Ethical Clearance: The project was approved by the local ethical committee in University of Baghdad.

Authors' Contribution Statement

S. N. M. and H. H. A., contributed to the design and implementation of the research to the analysis of the results and to the writing of the manuscript

References

1. Burger M, Skočić M, Bukvić S. Study of self-absorption in laser induced breakdown spectroscopy. Spectrochim Acta B: At. Spectrosc. 2014; 101: 51-56. https://doi.org/10.1016/j.sab.2014.07.007 .
2. Majeed NF, Naeemah M R, Ali AH. Spectroscopic analysis of clove plasma parameters using optical emission spectroscopy. Iraqi J Sci. 2021; 62(8): 2565–2570. https://doi.org/10.24996/ijs.2021.62.8.9 .

3. Ahghari M R, Soltaninejad V, Maleki A. Synthesis of nickel nanoparticles by a green and convenient method as a magnetic mirror with antibacterial activities. Sci Rep. 2020; 10: 12627. https://doi.org/10.1038/s41598-020-69679-4.
4. Abdalameer NK, Jassim RH, Jebur EK, Mazhir SN. Laser pulse's frequency effect on plasma parameters for titanium dioxide produced by FHG of a Q-Switched Nd: YAG pulse laser. Int J Nanosci. 2023; 21(2): 1-7. https://doi.org/10.1142/S0219581X23500114.
5. Sadaa AM, Al Abdullah ZT. Green Synthesis of Nickel Nanoparticles and their Application of Removal of Aliphatic Hydrocarbons from Crude Oil. Iraqi J Sci. 2021; 62(11): 4333–4341. https://doi.org/10.24996/ijs.2021.62.11(SI).14.
6. Qasim S A, Mazhir SN. Spectroscopic Analysis Of ZnO:Fe_3O_4 Using Laser-InducedBreakdown Spectroscopy. AIP Conf Proc. 2023; 2475: 090011. https://doi.org/10.1063/5.0104215.
7. Khan Z H, Ullah H M, Rahman B, Talukder A I, Abedin K M, Haider A F. Laser-Induced Breakdown Spectroscopy (LIBS) for Trace Element Detection: A Review. J Spectrosc. 2022; 2022 3887038. https://doi.org/10.1155/2022/3887038 .
8. Yaseen W I, Ahmed A F, Alshakarchi D, Muliak F. Development of a high-power LC circuit for generating arc plasma and diagnostic via optical emission spectroscopy. Appl Phys A. 2022; 128(2): 148. http://dx.doi.org/10.1007/s00339-022-05301-w .
9. Yahya K A, Rasheed B F. Effects of Discharge Current and Target Thickness in Dc -Magnetron Sputtering on Grain Size of Copper Deposited Samples. Baghdad Sci J. 2019; 16(1): 84-87. http://dx.doi.org/10.21123/bsj.2019.16.1.0084.
10. Mazhir S N, Abdullah N A, Rauuf A F, Ali A H, Al-Ahmed H. Effects of Gas Flow on Spectral Properties of Plasma Jet Induced by Microwave. Baghdad Sci J. 2018; 15(1): 81-86. https://doi.org/10.21123/bsj.2018.15.1.0081 .
11. Naeema N, Kudher A, Mohammed G. Study of the Spectroscopic Performance of Laser Produced CdTe, and CdTe:Ag Plasma. IOP Conf Ser Mater Sci Eng. 2020; 757, 012025. https://doi.org/10.1088/1757-899X/757/1/012025
12. Abdalameer N Kh, Mazhir S N. Laser-Induced Plasma Atomic and Ionic Emission during Target Ablation. Int J Nanosci. 2021; 20(5): 1–8. https://doi.org/10.1142/S0219581X21500447 .
13. National Institute of Standards and Technology. Atomic spectra database DB/OL. 2017. https://www.nist.gov/pml/atomic-spectra-database.
14. Shehab M M. Using Boltzmann Plots Method to Calculate Plasma Parameters Generated from a Magnesium Target Using Optical Emission Spectroscopy Technique. Int J Nanosci. 2022; 21(4), 2250029. https://doi.org/10.1142/S0219581X22500296 .
15. Singh JP, Thakur SN. Laser-Induced Breakdown Spectroscopy. 1st Edition (Elsevier Science, 2007.
16. Raja I LP, Valanarasub S, Isaac R S R, Ramudud M, Bitlae A. The role of silver doping in tuning the optical absorption, energy gap, photoluminescence properties of NiO thin films for UV photosensor applications. Optik. 2022; 254: 168634. https://doi.org/10.1016/j.ijleo.2022.168634 .
17. Zarenezhad E, Abdulabbas H.T, Marzi M, Ghazy E, Ekrahi M, Pezeshki B, Ghasemian A, Moawad AA. Nickel Nanoparticles: Applications and Antimicrobial Role against Methicillin-Resistant Staphylococcus aureus Infections. Antibiotics (Basel). 2022; 11(9):1208. https://doi.org/10.3390/antibiotics11091208 .
18. Fikry M, Tawfk W, Omar M M. Investigation on the effects of laser parameters on the plasma profile of copper using picosecond laser induced plasma spectroscopy. Opt Quant Electron. 2020; 52**:** 249. https://doi.org/10.1007/s11082-020-02381-x .
19. Wiese W L, Fuhr J R, Lesage A. Experimental Stark Widths and Shifts for Spectral Lines of Neutral and Ionized Atoms (A Critical Review of Selected Data for the Period 1989 through 2000. J Phys Chem Ref Data. 2020; 31(3): 819-927. https://doi.org/10.1063/1.1486456 .

2024, 21(5): 1684-1691
https://dx.doi.org/10.21123/bsj.2023.8327
P-ISSN: 2078-8665 - E-ISSN: 2411-7986
Baghdad Science Journal

تأثير طاقة الليزر النبضي على خصائص بلازما النيكل المنتجة بنظام البلازما المحتثة بالليزر

صباح نوري مزهر، هدى حسين عباس

قسم الفيزياء، كلية العلوم للبنات، جامعة بغداد، العراق

الخلاصة

تُستخدم تقنية قياس طيف الانبعاث البصري (OES) لتحليل البلازما المتولدة من هدف (النيكل) المضاء باستخدام ليزر Q- Switched (Nd: YAG) بطاقات مختلفة في الهواء. تم استخدام طريقة التوسيع Boltzmann-Plot و Stark لحساب معاملات البلازما بما في ذلك كثافة الإلكترون (n_e) ودرجة حرارة الإلكترون (T_e) وتردد البلازما (f_p) وطول ديباي (λ_D). يتضح أن قيم (n_e) و (T_e) و (λ_D) و (f_p) تزداد بزيادة طاقة الليزر مع قيم درجة حرارة الإلكترون المحسوبة التي تتراوح بين (0.934 - 1.479) الكترون - فولت.

الكلمات المفتاحية: طول ديباي، درجة حرارة الالكترون، النيكل، التحليل الطيفي المستحث بالليزر،البلازما.